Investigation of manufacturing process effects on microstructure and fatigue prediction in composite automotive tailgate design

Joseph Fitoussi, Samia Nouira, Khaled Benfriha, Mohamed-Amine Laribi, Achraf Kallel, Robert Tie Bi, Mohammadali Shirinbayan

ORIGINAL ARTICLE

Investigation of manufacturing process effects on microstructure and fatigue prediction in composite automotive tailgate design

Joseph Fitoussi[1] · Samia Nouira[1] · Khaled Benfriha[2] · Mohamed Amine Laribi[3] · Achraf Kallel[4] · Robert Tie Bi[5] · Mohammadali Shirinbayan[1]

Abstract

Manufacturing processes significantly influence microstructural variations in short fiber reinforced composites, which affect damage characteristics and fatigue life. Accurate fatigue life prediction is critical, especially when considering the impact of these manufacturing induced microstructural nuances. In this study, we investigate how manufacturing processes shape microstructures and their impact on fatigue life prediction. We present an advanced micromechanical model for predicting fatigue life in tangible structures, considering the microstructure distribution influenced by manufacturing dynamics. Our model links damage from monotonic loading to fatigue life, resulting in a multi-scale fatigue prediction model. This approach builds a database revealing the interaction between Tsai-Wu failure criterion parameters, manufacturing-induced microstructural variations, and target fatigue life. Using these insights, we fine-tune material properties in finite element simulations for precise design optimization. We illustrate our method using an automotive tailgate made from a sheet molding compound. This research highlights the critical role of manufacturing processes in microstructure variation and fatigue life prediction. It offers the potential for significant vehicle weight reduction, energy savings, and reduced emissions in automotive design and promises to be a valuable tool for optimizing manufacturing process parameters.

Keywords Fiber-reinforced composite modeling · Structure design · Micromechanics · Fatigue life prediction

1 Introduction

Due to their exceptional adaptability, enabling the exploitation of the unique properties of their constituent materials, composites have established a wide range of practical applications. In particular, short fiber reinforced composites (SFRCs) have gained prominence in high-volume automotive applications due to their geometric versatility and significantly reduced manufacturing time.

This study focuses on a specific category of discontinuous fiber-reinforced polymers, namely sheet molding compound (SMC) composites, supplied by FAURECIA Automotive.

✉ Mohammadali Shirinbayan
mohammadali.shirinbayan@ensam.eu

Joseph Fitoussi
joseph.fitoussi@ensam.eu

Samia Nouira
samia.nouira@ensam.eu

Khaled Benfriha
khaled.benfriha@ensam.eu

Mohamed Amine Laribi
a.laribi@estia.fr

Achraf Kallel
achraf.kallel@devinci.fr

Robert Tie Bi
robert.tiebi@forvia.com

[1] Arts Et Metiers Institute of Technology, CNAM, CNRS, PIMM, HESAM University, 75013 Paris, France

[2] Arts Et Metiers Institute of Technology, CNAM, LCPI, HESAM University, 75013 Paris, France

[3] University of Bordeaux, ESTIA Institut de Technologie, Technopôle Izarbel, 64210 Bidart, France

[4] Léonard de Vinci Pôle Universitaire, Research Center, La Défense, 92916 Paris, France

[5] Zero Emission, FORVIA Clean Mobility, Bois Sur Prés, 25550 Bavans, France

SMC composites find extensive application in automotive structural components like underbody structures, windscreen surrounds, and suspension arms. The microstructure of these composites is inherently molded during the compression of fiber pre-impregnated sheets, marked by substantial material flow dynamics. This molding process results in unique fiber orientation distributions, heavily impacted by the complexities of the mold geometry.

Therefore, real SMC (sheet molding compound) composite components showcase diverse microstructures, exhibiting notable variability across various points within the structure. This diversity results in considerable spatial differences in mechanical properties within composite structures. Hence, a precise comprehension of the spatial arrangement of these microstructures becomes indispensable for efficient structural design. Insufficient management of fiber orientation may result in the formation of weak zones within the structure. Conversely, optimizing microstructures holds the potential to substantially enhance component performance [1–5].

Therefore, accurate and efficient prediction of the anisotropic, inhomogeneous, and process-dependent mechanical properties is crucial. Such predictions can provide tangible benefits, including the reduction of costly prototyping efforts and streamlined development cycles, thereby optimizing structural design and promoting economic efficiency. In addition, effective design requires a comprehensive understanding of the complex interactions between individual components and their collective effect on the overall behavior of the composite. In this context, multi-scale damage analysis becomes essential. In particular, Meraghni et al. [6] conducted an investigation of damage propagation in discontinuous, randomly oriented fiber-reinforced composites. Their experimental investigation, based on microscopic observations and acoustic emission analysis, revealed two primary damage mechanisms: fiber-matrix interface degradation and matrix microcracking. Several other researchers [7–9] agree that fiber-matrix interface debonding is typically the primary damage mechanism, with matrix microcracking following closely behind in SMC composites. However, the experimental characterization of interfacial debonding presents significant challenges. To address this, Fitoussi et al. [10] conducted specific experiments on SMC composites. In contrast, Jendli et al. [7, 11] have been working in the field of interrupted and monotonic tensile testing and have provided a comprehensive range of qualitative and quantitative insights into the effect of strain rate on damage thresholds and kinetics. They introduced the innovative concept of "visco-damage," which is characterized by an increase in the strength of the fiber-matrix interface as the strain rate escalates. Remarkably, congruent results were subsequently substantiated by Fitoussi et al. [9] and Shirinbayan et al. [12], particularly for materials with analogous properties. Collectively, these studies comprehensively clarify the intricate mechanisms governing damage in SMC composites, offering invaluable insights essential for optimizing their structural design and enhancing performance. Reliable models must encompass microscopic phenomena such as damage and recognize the microstructure as a key input for predicting behavior laws and establishing boundary criteria for finite element structural calculations [13, 14]. To this end, mean-field homogenization methods provide an appropriate solution. Fitoussi et al. [15–17] proposed a micromechanical model for fiber/matrix debonding using an anisotropic equivalent inhomogeneity approach for damaged fibers, incorporating a probabilistic fiber-matrix interface. In a parallel vein, Meraghni et al. [18] introduced a similar model that links fiber/matrix debonding interfaces to a microcrack density parameter. In addition, Derrien et al. [19] extended the probabilistic interface damage model introduced by Fitoussi et al. [17] by experimentally validating the approach of replacing damaged fibers with an equivalent volume of matrix or inhomogeneity. Desrumaux et al. [20] adopted a statistical representation of failure for each component (fibers, matrix, and fiber/matrix interface). Subsequently, Meraghni et al. [21] developed a probabilistic strength model. In a different approach, Desrumaux et al. [22] proposed a two-stage homogenization damage model based on the numerical determination of the Eshelby tensor. A parallel two-step homogenization framework was outlined by Jendli et al. [23]. Kammoun et al. [24] introduced models for fiber/matrix interface decohesion within pseudo-grain sub-regions. Similarly, Guo et al. [25] introduced a damageable elastic law for randomly reinforced composites based on a two-scale approach. Nguyen et al. [26] presented a matrix degradation model based on the experimental research of Meraghni and Benzeggagh [6]. Baptiste [27] developed a model to describe the inelastic mechanical behavior of a composite, including viscosity, plasticity, and damage. Local damage is considered using the probabilistic interface decohesion approach developed by Fitoussi et al. [17]. Yang et al. [28] suggested a phenomenological damage approach that relies on two coupled damage parameters to distinguish interface debonding and matrix cracking. This involves the use of a von Mises criterion and a cohesive zone model to capture both damage mechanisms. Notta-Cuvier et al. [29] proposed a model based on void accumulation and phenomenological parameters to elucidate interface debonding at fiber head surfaces in injection-molded SFRC composites.

Additionally, predicting fatigue life while considering damage evolution in SFRC (steel fiber reinforced concrete) material stands as a pivotal concern in automotive structural design. Fatigue damage can also be characterized using local damage criteria or laws [30, 31], wherein parameters are contingent upon the number of applied cycles. Ben Cheikh Larbi et al. [8] studied the elastic behavior of SMC composites under fatigue loading. They

found suitable parameters for the two-scale damage probabilistic model by analyzing cyclic tests via scanning electron microscopy. Other advanced modeling approaches, based on damage mechanics, were also proposed for SFRC progressive failure of the material. As an example, the model of Nouri et al. [32] takes into consideration the material anisotropy via a macroscopic-anisotropic damage approach. It was employed to reproduce the experimental damage of SFRC polyamide 6 [33–35]. Damage is introduced through five internal state parameters. The main limitation of this type of model is the insensitivity to the loading rate and to the microstructure which makes it difficult to use in the case of real complex loading.

Furthermore, the prediction of fatigue life, accounting for damage evolution in short fiber reinforced composite (SFRC) materials, stands out as a paramount challenge in the domain of automotive structural design. Fatigue-induced damage can be elucidated through the lens of local damage criteria or local damage laws [30, 31] where parameters are contingent upon the number of applied cycles.

Ben Cheikh Larbi et al. [8] conducted a meticulous examination of the elastic behavior of SMC composites under fatigue loading. Through a rigorous analysis of cyclic tests employing scanning electron microscopy, they identified pertinent parameters for a two-scale damage probabilistic model. Additionally, advanced modeling approaches, grounded in damage mechanics, have been proposed to elucidate the progressive failure of SFRC materials. Notably, Nouri et al.'s model [32] incorporates material anisotropy through a macroscopic-anisotropic damage approach. This model has been effectively employed to replicate experimental damage observations in SFRC polyamide 6 [33–35] where damage is characterized by five internal state parameters.

Nevertheless, these models exhibit a key limitation in their insensitivity to loading rates and microstructural intricacies, rendering them less practical for applications involving complex real-world loading scenarios.

Moreover, material cards employed in finite element structural design encompass a failure criterion; the determination of which proves challenging in the case of anisotropic materials. In the literature, numerous approaches based on failure criteria for SFRCs under cyclic loading have been proposed. These approaches often draw inspiration from criteria developed for metallic materials. However, the pronounced anisotropy inherent in SFRC materials significantly impacts fatigue failure, rendering traditional isotropic and homogeneous criteria, designed primarily for metals, inadequately predictive. Consequently, in the context of actual SFRC structures characterized by substantial microstructural variations, establishing the corresponding spatial distribution of the failure criterion presents a formidable undertaking.

In this paper, the focus encompasses two primary areas: "Material, Microstructure Variability and Structural Implications" and "SMC Damage Behavior Characterization." Firstly, Section 2 on "Material, Microstructure Variability, and Structural Implications" delves into the intricate relationship between materials and their microstructural variations within SMC components. This section aims to elucidate the significant implications these variations hold for the overall structural integrity, emphasizing the spatial differences in mechanical properties within composite structures. Subsequently, Section 3 dedicated to "SMC Damage Behavior Characterization" delves into a comprehensive analysis of the behavior exhibited by SMC materials under varying stress and fatigue conditions. This part aims to provide insights into how SMC materials respond to damage, particularly focusing on their fatigue life and stiffness reduction after cycling.

In this study, we present a multi-scale fatigue life prediction framework capable of handling complex loading scenarios while accommodating the variable microstructure found in real-world automotive short fiber reinforced composite (SFRC) structures. Using a multi-scale damage model based on the Mori and Tanaka approach, we establish a Tsai-Wu failure criterion database that accounts for microstructural variations and the number of loading cycles.

We illustrate the utility of this approach by applying it to the analysis of an SMC tailgate, generously provided by Faurecia for the PSA 3008 car. Through this analysis, we identify opportunities to optimize design and process parameters. This optimization process serves the dual purpose of reducing structural weight while meeting stringent fatigue life requirements, thus improving both efficiency and durability in automotive design.

2 Material, microstructure variability, and structural implications

2.1 Material

The material investigated in this study is a conventional sheet molding compound (SMC), which is widely used in the manufacture of PSA 3008 tailgates. SMC is supplied in its partially processed state as preformed sheets of glass-fiber-reinforced polyester, primarily for compression molding applications. These sheets are produced by dispersing 25-mm long chopped glass fibers, organized in bundles of approximately 200 fibers each, in a bath of polyester resin enriched with calcium carbonate particles. The resulting sheets are then wound into rolls and cut into batches. These charges are then placed in a mold, which is heated to the glass transition temperature, allowing an optimized cycle time of approximately 1 min.

Throughout the compression molding process, the dynamic material flow characteristics facilitate the production of parts that are close to the net shape, even with complex geometries. However, it is important to emphasize that the extended fiber length present in SMC composites gives them increased strength properties, while at the same time introducing notable property variations at different locations, mainly due to the intricate interplay of material flow dynamics.

2.2 Ultrasonic measurements

Given the profound impact of microstructural attributes on both material strength and fatigue life, it becomes imperative to delve into the intricate dispersion of microstructures within real-world SMC composite structures. To accomplish this task, a straightforward ultrasonic method, as elucidated in references [4, 36] can be effectively employed. In this technique, ultrasonic shear waves are systematically generated to traverse the specimen's width along a predefined plane, dictated by the Snell-Descartes law. Multiple rotations are executed to construct a comprehensive depiction of the fiber orientation distribution within the specimen (for detailed methodology, refer to [4, 36]).

Various samples are strategically extracted from distinct locations within the tailgate to evaluate their respective average microstructures. Subsequently, a cartographic representation delineating the spatial distribution of microstructures within the composite structure is meticulously crafted. For visual elucidation, Fig. 1 acts as an illustrative representation, displaying the microstructure distribution revealed by ultrasonic analysis. Within the cross-section of a PSA 3008 tailgate, the red line's orientation indicates the primary alignment of reinforcements, with its length indicating the strength or intensity of this alignment. Consequently, a circular representation conveys a randomized orientation. It is worth noting that, for comparative purposes, the microstructural heterogeneity observed within SMC structures markedly surpasses that found in injection-molded thermoplastic matrix composite structures. To a somewhat lesser extent, this variability is also discernible within a sheet exclusively prepared for the purposes of this investigation.

For SMC composites, the anisotropic stiffness tensor can be predicted as a function of microstructure by incorporating the subsequent orientation distribution function into a Mori and Tanaka model:

$$\frac{f^{\theta}}{f} = \frac{k}{n} * \left(1 + M * \cos\left(2\left(\theta - \theta_P\right)\right)\right) \tag{1}$$

where f^{θ} and f represent the volume fraction of fibers aligned at θ_P (corresponding to the main material flow direction during manufacturing) and the total fiber volume fraction, respectively. The parameter n denotes the number of orientation families included in the Mori and Tanaka approach, and M indicates the fiber orientation rate. It is worth noting that this parameter exhibits a direct proportional relationship with the acoustic birefringence coefficient, referred to as K% (as detailed in references [4, 37]). This coefficient, in turn, is associated with the fiber orientation rate, designated as M. The determination of this coefficient relies on the ultrasonic method previously described. The specific proportionality constant is ascertained through meticulous analysis of numerous well-defined microstructures extracted from both sheet materials and actual components. Subsequently, the parameter "k" is adjusted in accordance. It should be emphasized that this function has been empirically shown to be a highly reliable representation of SMC composites, as confirmed in the literature [4, 36]. As a result, the derived values of M% and primary fiber orientation at each location can be effectively used to formulate quantitative cartographic representations of the microstructures within the tailgate, as illustrated in Fig. 2.

3 SMC damage behavior characterization

Monotonic tensile tests were conducted under quasi-static loading conditions. These mechanical evaluations were executed on a meticulously chosen array of microstructures, employing the specimen selection methodology expounded upon in [38].

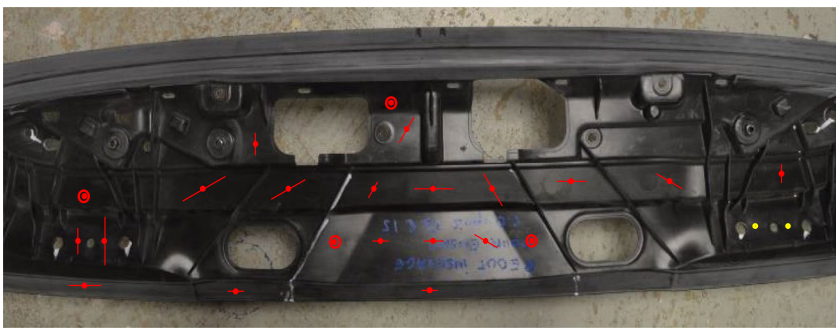

Fig. 1 Spatial microstructure mapping in a section of an SMC tailgate [4, 36]

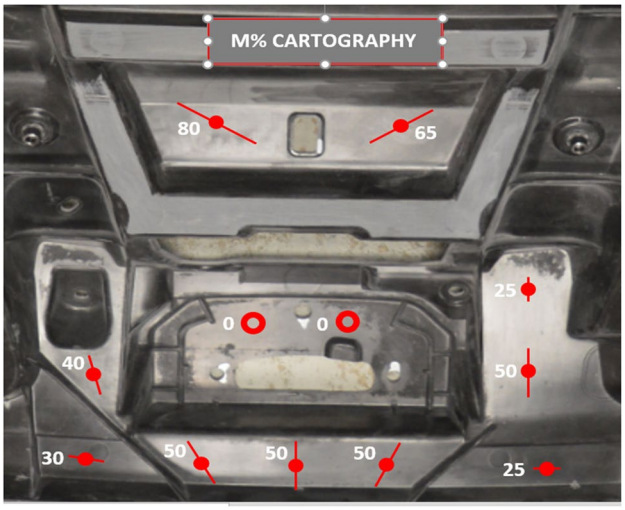

Fig. 2 Real spatial microstructure distribution, as determined through ultrasonic measurements performed at the tailgate lock position

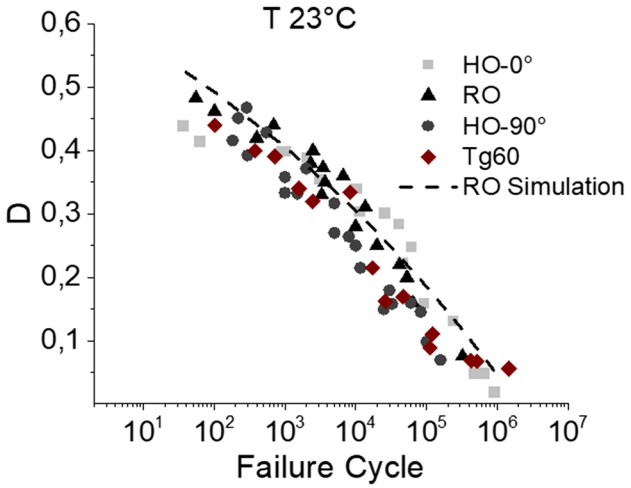

Fig. 3 Intrinsic relation D-Nr

To examine the gradual degradation of stiffness during tensile loading, a sequence of load-unload tensile test was conducted, following the comprehensive procedure outlined in [30, 38]. Subsequently, the macroscopic damage parameter, as per the definition provided by Kachanov [37], was graphically represented (refer to Fig. 5):$D = 1 - \left(\frac{E}{E_0}\right)$.

Tension-tension fatigue tests were also carried out at various maximum applied stress levels. These assessments were carried out at an operating frequency (f) of 10 Hz and a stress ratio (R) of 0.1. Each fatigue test was preceded by a quasi-static tensile load-unload-elastic reloading cycle. Consequently, for each fatigue test, the stiffness loss of the first cycle was systematically evaluated using the macroscopic damage parameter after the first cycle:$D_1 = 1 - \left(\frac{E_1}{E_0}\right)$ where E_0 is Young's modulus of the material in the unloaded state, and E_1 is the residual Young modulus at the end of the initial cycle.

4 Micromechanical microstructure-dependent fatigue life prediction

4.1 Fatigue life prediction methodology

In earlier publications [38, 39], it was demonstrated that fatigue life correlates with the decrease in stiffness following the initial cycle. Notably, this correlation remains unchanged regardless of microstructural parameters (M%, θ_P). It is worth noting that this relationship has recently been verified and employed in the context of thermoplastic matrix materials [40]. Figure 3 underscores this correlation across four distinct microstructure configurations: HO and RO denote highly oriented and randomly oriented microstructures, respectively. HO-0° and HO-90° correspond to results derived from specimens aligned at 0° and 90° concerning the fatigue tensile direction. Tg60 refers to specimens extracted from the quality control zone of the PSA 3008 tailgate where the fibers in these samples are oriented at a 60° angle relative to the loading direction.

As a result, the mathematical formulation of this inherent relationship makes it easy to predict the S–N curves by means of the following equation:

$$N = \left(\frac{1 - D_S}{C}\right)^{\frac{1}{P}} \tag{2}$$

where N is the number of cycles to failure under an applied macroscopic tensile stress, S. D_S is the reduction in stiffness after the first cycle. The material parameters C and P should be determined from the results obtained from the RO microstructure.

Therefore, for any other microstructure configuration, $\mu^i = (M\%, \theta_P)^i$, the prediction of D_S as a function of S gives access to the corresponding S–N curve. Figure 4 summarizes graphically the different stages of the micromechanical microstructure-dependent fatigue life prediction methodology discussed in paragraph 3. See also [38] for a step-by-step description. However, a micromechanical damage model for monotonic loading is needed. The latter is described in the next paragraph.

Therefore, for any alternative microstructure configuration, denoted as $\mu^i = (M\%, \theta_P)^i$, the estimation of D_S as a function of S provides the means to access the corresponding S–N curve. Figure 4 provides a visual summary of the various stages involved in the micromechanical, microstructure-dependent fatigue life prediction methodology described in Section 3. A step-by-step description can be found in [38].

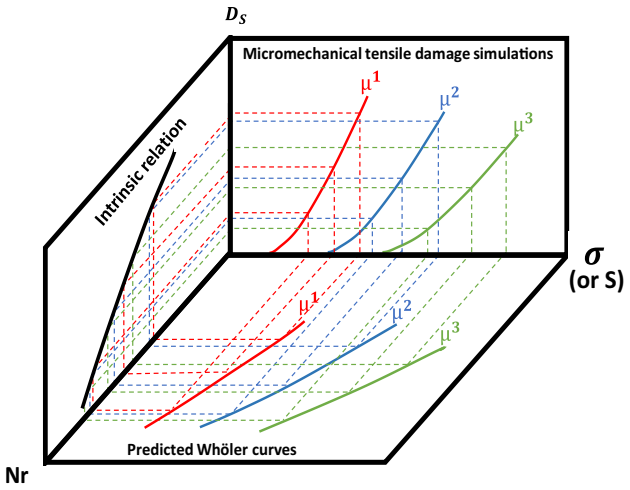

Fig. 4 Micromechanical microstructure-dependent fatigue life prediction

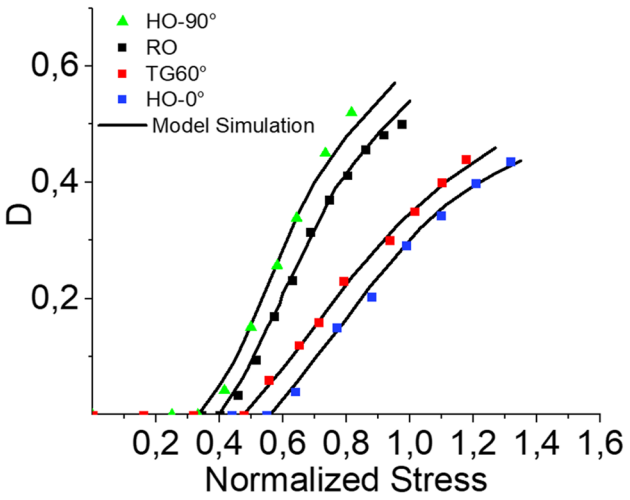

Fig. 5 Comparison between experimental and predicted damage parameter evolution

However, it is important to note that an efficient micromechanical damage model for monotonic loading is essential and will be discussed in the following section.

4.2 Micromechanical damage prediction model

The aim of this paragraph is to briefly describe a micromechanical damage model for monotonic loading which should be used in the fatigue life prediction method mentioned in the previous paragraph. More specifically, the prediction of D_S as a function of S for any targeted microstructure configuration, $\mu^i = (M\%, \theta_P)^i$ to realize the corresponding S–N curve.

It has been shown that the fiber-matrix interface failure is the main local damage mechanism. This has been verified in the case of monotonic quasi-static, monotonic dynamic, and cyclic [23, 41, 42] loadings.

In the case of monotonic loading, debonding criteria using a combination of damage criteria and the Weibull distribution has been frequently used [19, 22, 43–46]. In this work, we use the following formulation [16, 23, 30].

The purpose of this section is to provide a concise description of a micromechanical damage model designed for monotonic loading. This model is intended for use in the fatigue life prediction methodology outlined in the preceding section, specifically for predicting D_S as a function of S for any targeted microstructure configuration denoted as $\mu^i = (M\%, \theta_P)^i$ to derive the corresponding S–N curve.

Extensive evidence has indicated that the primary local damage mechanism involves fiber-matrix interface failure. This observation has been corroborated across a range of loading conditions, including monotonic quasi-static, monotonic dynamic, and cyclic loadings [23, 41, 42]. In the case of monotonic loading, debonding criteria have frequently been applied, utilizing a combination of damage criteria and the Weibull distribution, as demonstrated in prior studies [19, 22, 43–46]. In this research, we adopt the following formulation, as described in [16, 23, 30]:

$$P_r = 1 - \exp\left(-\left(\left(\frac{\sigma}{\sigma_0}\right)^2 + \left(\frac{\tau}{\tau_0}\right)^2\right)^m\right) \quad (3)$$

P_r indicates the debonding probability calculated at the fiber-matrix interface. The local interface failure criterion corresponds to a quadratic combination of the local normal and shear stresses, σ and τ, respectively. σ_0 and τ_0 are the normal and shear strength at the interface, respectively.

The parameter "m" serves as a statistical factor designed to account for localized fluctuations in the microstructure. For a given microstructure denoted as $\mu^i = (M\%, \theta_P)^i$, the values of σ and τ and P_r can be computed for all fiber orientations using the Mori and Tanaka approach [47]. Specifically, at each stress increment, the damage model evaluates the maximum debonding probability for each fiber orientation, thereby considering the corresponding proportion of debonded fibers. The influence of local damage configuration, such as fiber and interfacial micro-cracks, is subsequently incorporated through the introduction of zero stiffness heterogeneity and a partial reduction in the stiffness participation of the debonded fibers. This reduction is reflected in a decrease in the fiber volume fraction for the given family of fiber orientations. As a result, at each loading step, a new microstructure is defined, encompassing three heterogeneity populations: non-damaged fibers, active fibers (comprising both non-damaged and partially damaged fibers), and micro-cracks. A two-step homogenization process is then executed to compute the residual composite stiffness tensor: the first stage involves homogenization of

the matrix and micro-cracks, followed by the introduction of fibers into the previously homogenized material in the second stage. For more comprehensive insights into the applied damage model, several references are available for consultation, including [23, 30].

Figure 5 illustrates the prediction of D_S for four specifically selected microstructure configurations, denoted as $\mu^i = (M\%, \theta_P)^i$. The strong agreement observed between the experimental and simulated curves serves to confirm the efficacy of the micromechanical model, thus substantiating its suitability for incorporation into the S–N curve prediction methodology.

4.3 Microstructure-dependent Wöhler curves abacus

Using the above methodology, it is possible to construct the Wöhler curve for any microstructure configuration, denoted as μ^i and defined by the pair $(M\%, \theta_P)^i$. Figure 6 shows an illustrative example of calculated Wöhler curves. Within this figure, each plot shows the progression of the calculated Wöhler curve for a particular microstructure defined by M% as a function of the primary fiber orientation, θ_P.

5 Novel approach for improved fatigue design in short fiber reinforced composite structures

The primary objective of this study is to introduce a methodology that enables the design and optimization of real automotive SFRC composite structures subjected to cyclic loading, taking into account the spatial distribution of the microstructure.

5.1 Methodology

To achieve this objective, the predicted Wöhler curves shown in Fig. 6 are used to identify an anisotropic failure criterion for each given microstructure configuration $\mu^i = (M\%, \theta_P)^i$ tailored to a specific number of cycles, N. It is important to emphasize that the primary fiber orientation parameter, $(\theta_P)^i$, is one of the local conditions directly managed by the finite element code. Consequently, the identified failure criterion should depend only on M% and N.

First, it is essential to establish both local and macroscopic coordinate systems, as shown in Fig. 7. For example, consider a representative volume element located

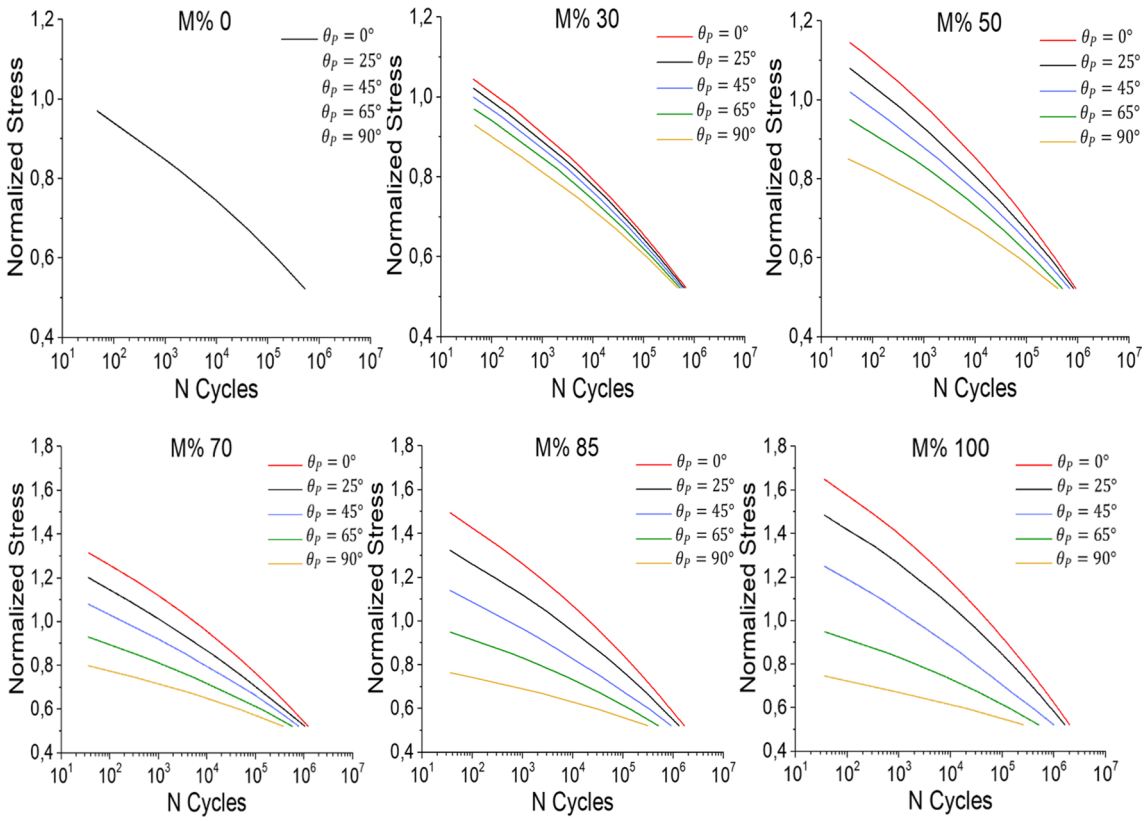

Fig. 6 Computed Wöhler versus microstructure

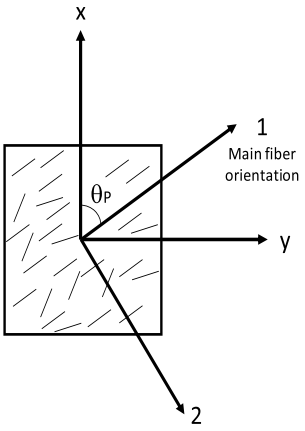

Fig. 7 Local and global coordinate systems

within the composite structure, characterized by a specific microstructure denoted μ^i and defined by a specific M% value. In this context, the local axis system (1,2) is aligned with the main fiber orientation direction (axis 1), while the (x, y) system corresponds to the macroscopic coordinates.

For a given cyclic tensile load, σ_X, applied in the x-direction, one can use the curves shown in Fig. 6 to plot the variation of σ_X as a function of θ_P for different numbers of cycles to failure, N (an example is shown in Fig. 8).

Previous studies [48, 49] have established the effectiveness of the Tsai-Wu criterion or the Tsai-Hill criterion in the prediction of the failure of short fiber reinforced composite materials. Assuming that failure stresses are in tension and compression (conservative approach), the two-dimensional formulation of the Tsai-Wu criterion in the context of thin structures submitted to pure tensile stress,σ_X, applied in the direction x requires that

$$\sigma_X < \left[\frac{1}{\frac{c^4}{X^2} + \frac{s^4}{Y^2} + c^2 s^2 \left(\frac{1}{S^2} + 2F_{12} \right)} \right]^{\frac{1}{2}} \tag{4}$$

where X, Y, and S are respectively the tensile failure stresses in directions 1, 2, and the in-plane shear failure stress. Note that in fatigue, there are functions of the applied number of cycles. Equation (3) is obtained after rotation of the stress tensor into the local coordinates (1, 2) where c and s denote $\cos(\theta_P)$ and $\sin(\theta_P)$, respectively. Moreover, it should be noted that the values of X and Y correspond to the values of σ_X for $\theta_P = 0°$ and $\theta_P = 90°$, respectively. Therefore, for a given number of cycles to failure, N, these values can be directly read in Fig. 8 (or an equivalent one obtained for any other value of M%). Consequently, only two unknown parameters, S and F_{12}, should be identified using an inverse method involving expression (9). See a result illustrated in Fig. 9 for $M = 60\%$ and fatigue life of 10^5 cycles. In this figure, S and F_{12} govern the form of the curve which should fit the evolution of the values directly checked from Fig. 6.

where X, Y, and S represent the tensile failure stresses in directions 1, 2, and the in-plane shear failure stress, respectively. It is important to note that, in the context of fatigue, these values are functions of the number of cycles applied. Equation (4) is derived following the rotation of the stress tensor into local coordinates (1, 2), where "c" and "s" represent $\cos(\theta_P)$ and $\sin(\theta_P)$, respectively. Furthermore, it should be emphasized that the values of X and Y correspond to the values of σ_X when $\theta_P = 0°$ and $\theta_P = 90°$, respectively. Consequently, for a given number of cycles to failure, N, these values can be taken directly from Fig. 8 (or

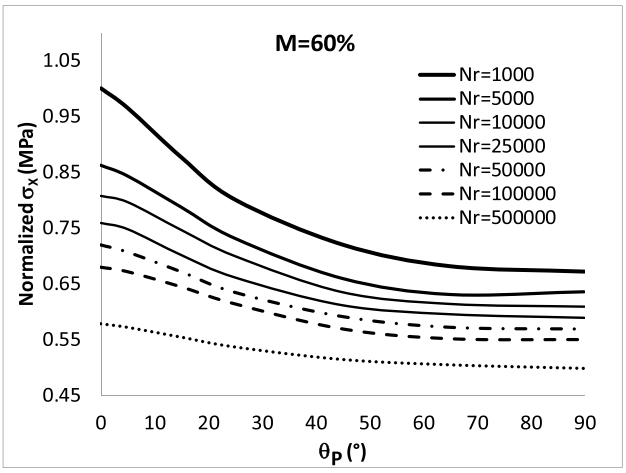

Fig. 8 Evolution of the tensile stress as a function of θ_P for the different number of cycles to failure (values checked from predicted abacus)

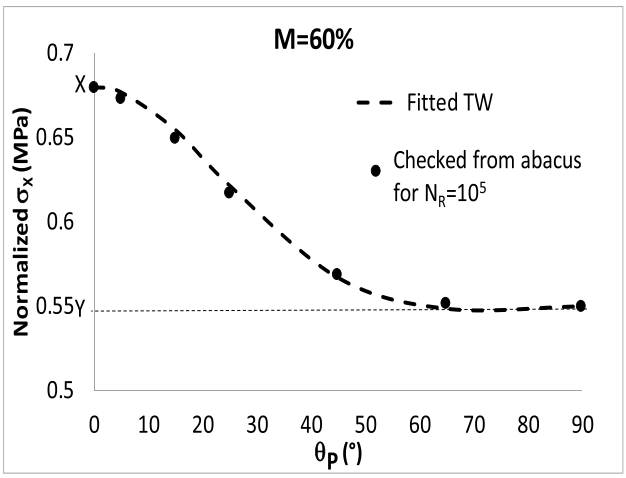

Fig. 9 Example of identification of Tsai-Wu parameters (X, Y, S, and $F12$) from expression (9) and Fig. 6 Wöhler curves

its equivalent for any other value of M%). As a result, only two unknown parameters, S and F_{12}, need to be determined using an inverse method involving expression (9). Figure 9 illustrates the results obtained for $M = 60\%$ and a fatigue life of 10^5 cycles. In this figure, S and F_{12} govern the shape of the curve, which should closely match the observed evolution of the values taken directly from Fig. 6.

This procedure should be repeated for any desired microstructure (M%) and fatigue life (N_R). A new abacus can therefore be constructed where the parameters of the Tsai-Wu criterion, X, Y, S, and $F12$, can be checked for any triggered number of cycles to failure. Some curves of this new abacus are shown in Fig. 10.

As a result, Fig. 11 illustrates the evolution of the Tsai-Wu criterion during cyclic loading for two different microstructural configurations: M% = 0% and M% = 100%, representing in plane randomly oriented fibers and highly oriented fibers, respectively. It is evident that in the case of

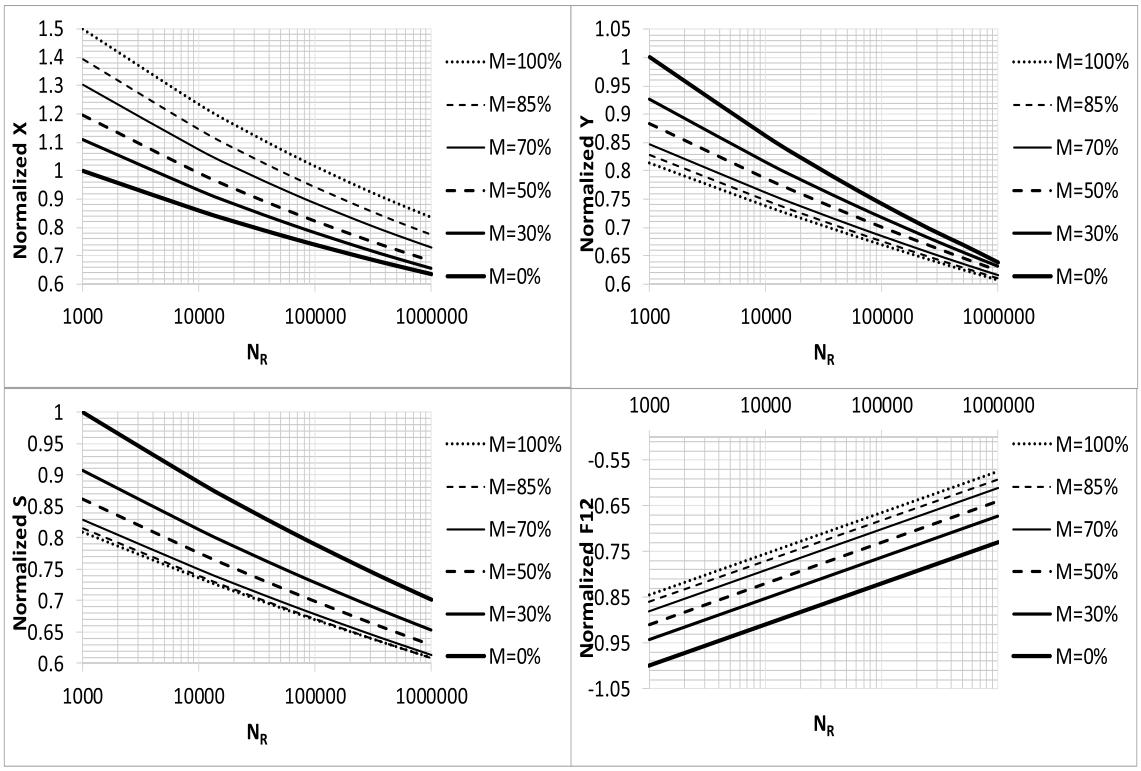

Fig. 10 Predicted abacus giving the evolution of the Tsai-Wu criterion parameters versus fatigue life and microstructure

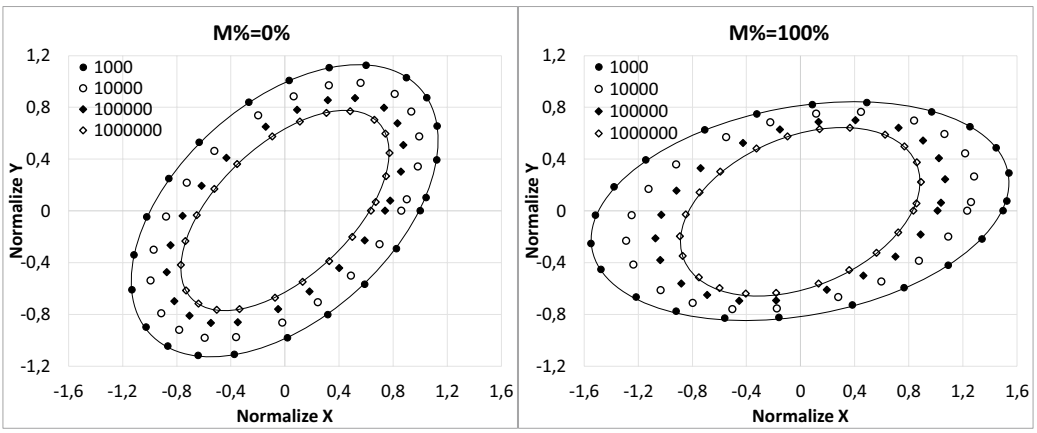

Fig. 11 Tsai-Wu criterion for a different targeted number of cycles and two typical microstructures

the highly oriented material, there is a discernible rotation of the Tsai-Wu surface. This transformation pattern indicates a gradual development of material anisotropy due to damage. In particular, the preferential fiber orientation in this scenario significantly influences the microcracking at the fiber-matrix interface in response to the stress state, resulting in a progressive change in the principal axis of anisotropy during fatigue. Conversely, in a randomly oriented material, progressive local damage is rapidly and uniformly distributed across all fiber orientations, resulting in a homothetic evolution of the failure criterion.

5.2 Case study on SMC tailgate

We will now present the potential for optimization of composite structures through the use of our newly developed abacus. Indeed, the abacus shown in Fig. 10 allows the evolution of the Tsai-Wu criterion during cyclic loading to be monitored for any SMC microstructure. Consequently, the failure criterion for a given stress state, microstructure, and desired fatigue life is known. These information allow the application of finite element analysis to determine the stress field distribution at each location where the microstructure is identified.

To illustrate the potential of the proposed methodology, we have chosen to focus on a particular area of an industrial tailgate (Peugeot 3008). Due to the elevated stress levels experienced by the material surrounding the tailgate lock, this region has been identified as a critical zone requiring optimization in terms of thickness, fiber orientation, and fatigue life. To this end, once the spatial distribution of the microstructure has been determined, an analysis of the associated stress state and Tsai-Wu criterion is carried out as a function of the number of tailgate opening and closing cycles. As will be shown below, the same tool can also be used to study the effect of the slamming speed. It is also possible to investigate the optimum thickness and local microstructure distribution.

5.2.1 Boundary conditions

Throughout its service life, the tailgate is subjected to impact velocities ranging from 0.25 to 2.5 m/s, depending on the user's behavior. Statistical analysis has shown that the velocity distribution follows a normal distribution with an average velocity of approximately 1.1 m/s. To allow for safety considerations, a standard impact velocity of 1.3 m/s is justified. In addition, finite element analysis (FEA), confirmed by physical measurements on the Peugeot 3008 tailgate, indicates that an average impact velocity of 1.3 m/s produces a force of 600 N in the lock zone. However, it is essential to take into account the repercussions of an applied force of 1500 N, which has a very low probability of occurring but which could result in significant damage.

To facilitate the analysis, a subsystem was extracted from the overall tailgate system under slamming conditions, and the appropriate boundary conditions were applied. Specifically, a displacement of 4.5 mm was imposed on the boundary nodes of the subsystem, as indicated by the white area in Fig. 12. This value corresponds to the average displacement observed in the global tailgate system during standard slamming events.

5.2.2 Material cards spatial distributions

In the following discussion, the spatial distribution of the microstructure as determined by ultrasonic measurements (Fig. 2) will be referred to as the "true microstructure." Observations reveal different microstructures with different levels of birefringence, corresponding to different orientation rates ranging from 0% (shown as circles) to 80% (shown as long double arrows) at different locations. Note that the relationship between M% and the birefringence parameter has been established by ultrasonic and mechanical measurements on RO, HO, and Tg60 microstructures in conjunction with the Mori and Tanaka elastic model.

Consequently, the anisotropic elasticity tensors were calculated for each M% value using the Mori and Tanaka elastic model, and the corresponding anisotropic stiffness tensors were assigned to their respective positions in the Abaqus finite element structure. The distribution of stress states is then calculated under conditions simulating a tailgate-slamming event (as detailed in the corresponding boundary conditions above). Using the Tsai-Wu parameters previously established in Abaqus (Fig. 10), it is possible to determine the failure criterion for any desired fatigue life and microstructure. Furthermore, the spatial material map used in finite element analysis is completed with the knowledge of the thickness distribution.

It should be noted that in regions far from the critical zone, the material is treated as randomly oriented. Finite element simulations have confirmed that the composite properties in these distant regions have a negligible influence on the resultant stress state.

5.3 Micromechanical finite elements analysis

5.3.1 Case studies

We aim to demonstrate how the results of our multi-scale approach can significantly contribute to a more comprehensive understanding and effective management of the influences of thickness, load amplitude, and microstructure distribution on the fatigue life of a real automotive structure. To achieve this, we have chosen to focus our analysis on the previously described lock fixation zone.

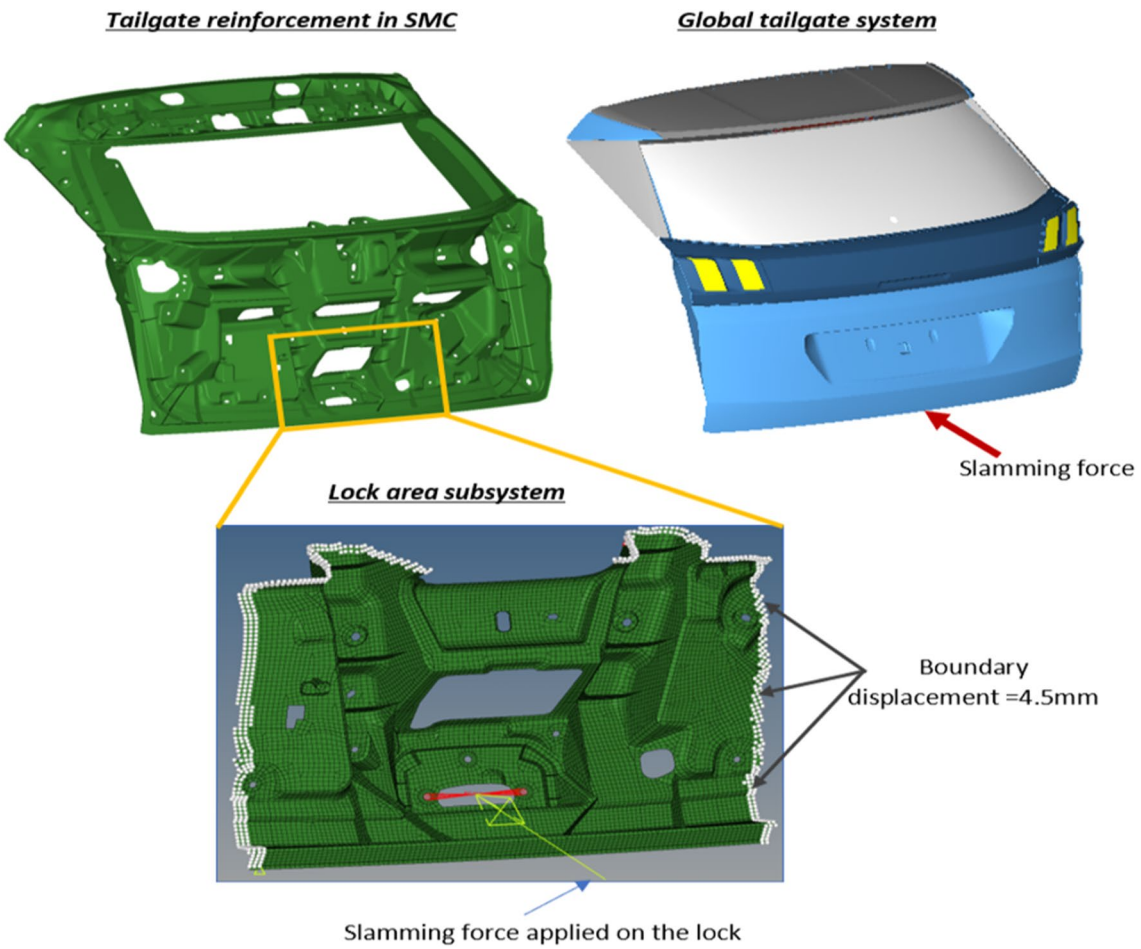

Fig. 12 Boundary conditions applied on the lock fixation zone subsystem

We have defined several spatial microstructure distributions for our investigation:

1. The actual microstructure (as shown in Fig. 2) serves as a valuable reference. First, we evaluate the effects of load amplitude and thickness in respect of this particular distribution of microstructure.
2. We then explore the influence of fiber orientation by examining different virtual spatial distributions (shown in Fig. 13). These configurations include scenarios where all fibers are oriented at 0°, and all fibers are oriented at 90°. A third configuration where fibers are oriented symmetrically at +45° and −45° is also considered. These configurations represent extreme cases and help to highlight the potential impact of material flow during thermoforming on fatigue life.

The spatial distributions of the corresponding material cards, including anisotropic stiffness tensors and the Tsai-Wu criterion, tailored to different required fatigue lives, are determined using the micromechanical approach outlined in Section 4.

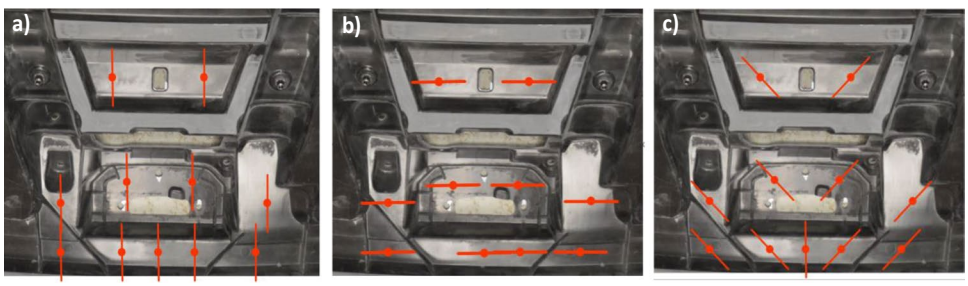

Fig. 13 Virtual spatial distributions. **a** all at 0°, **b** all at 90°, and **c** +-45° symmetric distribution

5.3.2 Effect of slamming speed

In accordance with the aforementioned boundary conditions and the spatial distribution of real material cards, our study initially focused on the application of a 600 N force (slamming at 1.3 m/s) to the lock fixation zone while also considering the occasional 1500 N load (slamming at 2.5 m/s). Figure 14 shows the calculated Tsai-Wu criterion field for different fatigue life scenarios. It is evident that three specific zones require careful analysis due to their higher failure criterion values: the lock fixation zones, the corner zones, and the stiffener zone (shown in Fig. 14). The graph shows the evolution of the Tsai-Wu criterion values during cyclic loading. However, under the conditions of a 1.3 m/s impact speed, relatively low values are observed even in these zones. For example, the corner zone shows a maximum value of 0.42 after 10^6 cycles. However, it is important to consider that repeated high-speed slamming at 2.5 m/s could significantly increase the vulnerability of the tailgate in the corner zones. Indeed, the evolution of the Tsai-Wu criterion in these areas during repeated slamming events is shown in Fig. 15, which indicates a value of 0.96 after 10^5 cycles at 2.5 m/s. It is also noteworthy that an increase in the rate of damage progression during fatigue is observed at higher slamming speeds. However, it must be emphasized that such slamming remains exceptional, and although it may affect fatigue life, it is extremely rare.

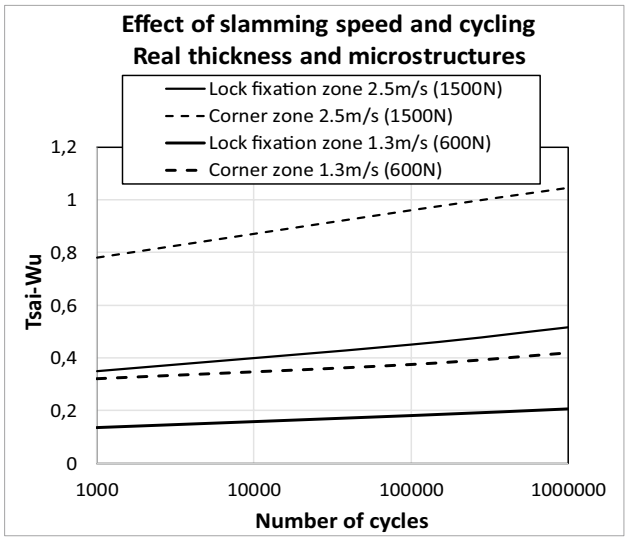

Fig. 15 Effect of slamming speed and cycling for the real microstructure on two critical zones

5.3.3 Effect of thickness

Figure 16 shows the Tsai-Wu fields computed for 10^5 cycles and different thickness reduction percentages, ranging from 20 to 50%, corresponding to weight reductions. As expected, the reduction in stiffness results in an increase

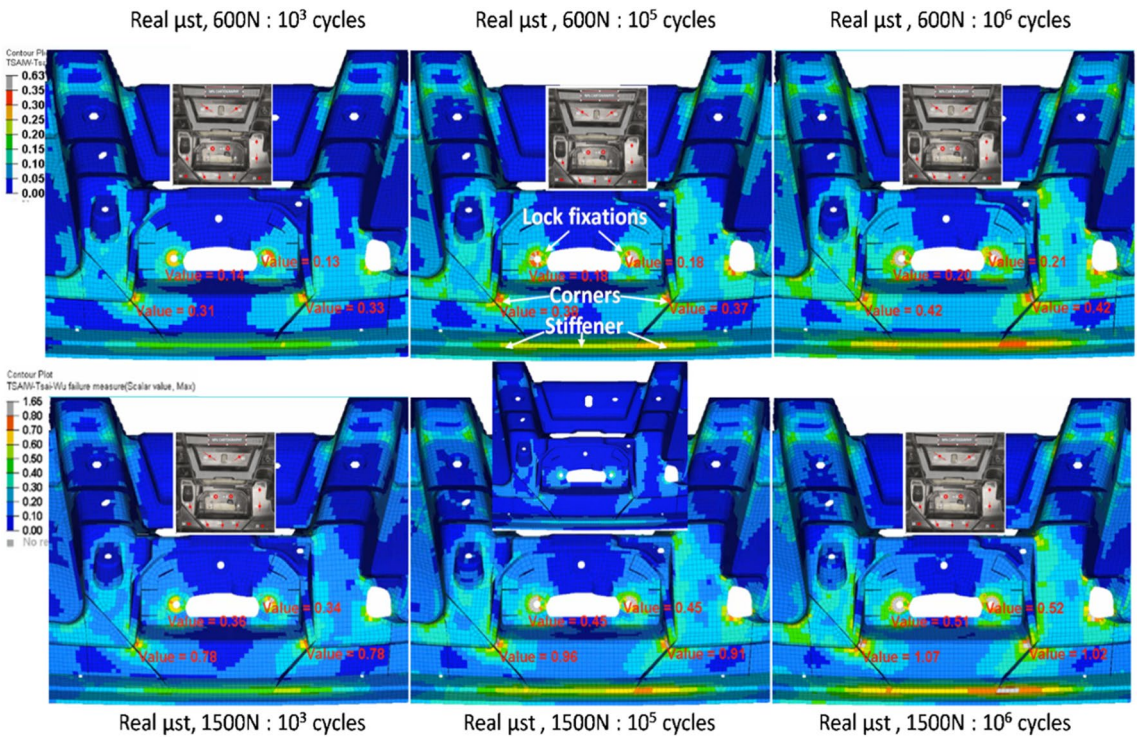

Fig. 14 Effect of slamming speed and cycling on the Tsai-Wu criterion distribution: real microstructures

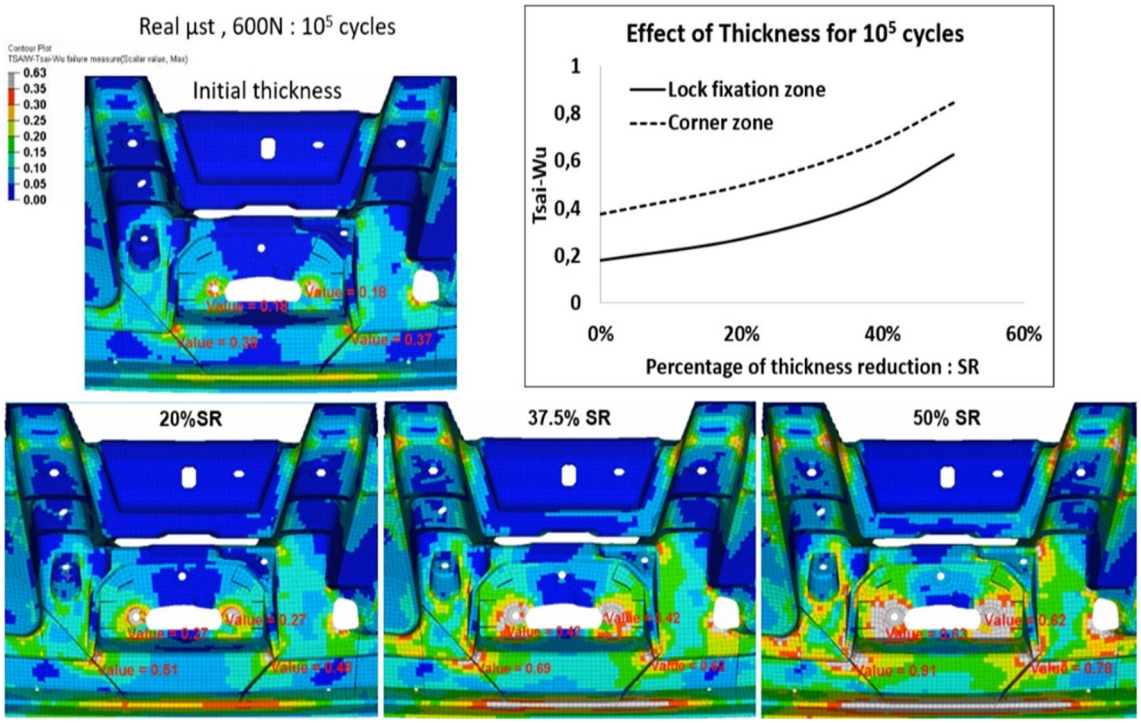

Fig. 16 Effect of stiffness on fatigue criterion at 10^5 cycles

in the Tsai-Wu criterion within the critical zones. In particular, there is an expansion of these critical zones. Furthermore, the evolution of the failure criterion as a function of thickness reduction is not linear, as might be expected in the absence of these results but follows an exponential trend. However, it is reasonable to propose a 20% thickness reduction, as this represents a significant optimization in the automotive industry.

5.3.4 Effect of orientation

To highlight the effect of fiber orientation, it is important to focus on a region where the stress is uniaxial. Such a scenario is provided by the stiffener zone discussed in Section 4.3.2 (see principal stress distribution in Fig. 17). The three case studies detailed in Section 4.3.1.b) were calculated using our prediction tool targeting a fatigue life of 10^5 cycles. The evolution of the failure criterion along the stiffener (indicated by the dotted zone) is shown in Fig. 17 for the three configurations.

Contrary to the prevailing expectation, modifying the spatial distribution of the fibers does not have a significant effect on fatigue failure. In fact, the maximum value of the Tsai-Wu criterion experiences only a marginal shift from 0.4 to 0.45, indicating a relatively minor effect. This result challenges the widely accepted notion in continuous fiber applications, such as laminates, that orienting fibers in the direction of the maximum principal stress will increase fatigue strength. In fact, an examination of the stress evolution shows that the changes in fiber orientation correspond to reorientations of principal stresses. The fatigue life is therefore not significantly affected (Fig. 18).

6 Conclusion

This study utilizes an original ultrasonic method to unveil distinct spatial variations in the microstructure of real automotive SMC composite structures. These variations primarily stem from material flow during thermocompression. Our investigations build upon prior multi-scale experimental analyses, emphasizing the substantial influence of microstructure on SMC damage behavior. Notably, our research reveals a consistent relationship between microscopic and macroscopic damage rates, irrespective of the mechanical loading type—monotonic or cyclic.

Furthermore, our methodology establishes a significant connection between monotonic damage and fatigue life, independent of microstructure. This paper introduces an innovative approach that integrates this intrinsic relationship with a predictive micromechanical damage model tailored for monotonic loading. This model enables the prediction of Wöhler curves based on microstructure, leading to microstructure-dependent S–N curves and a failure criterion

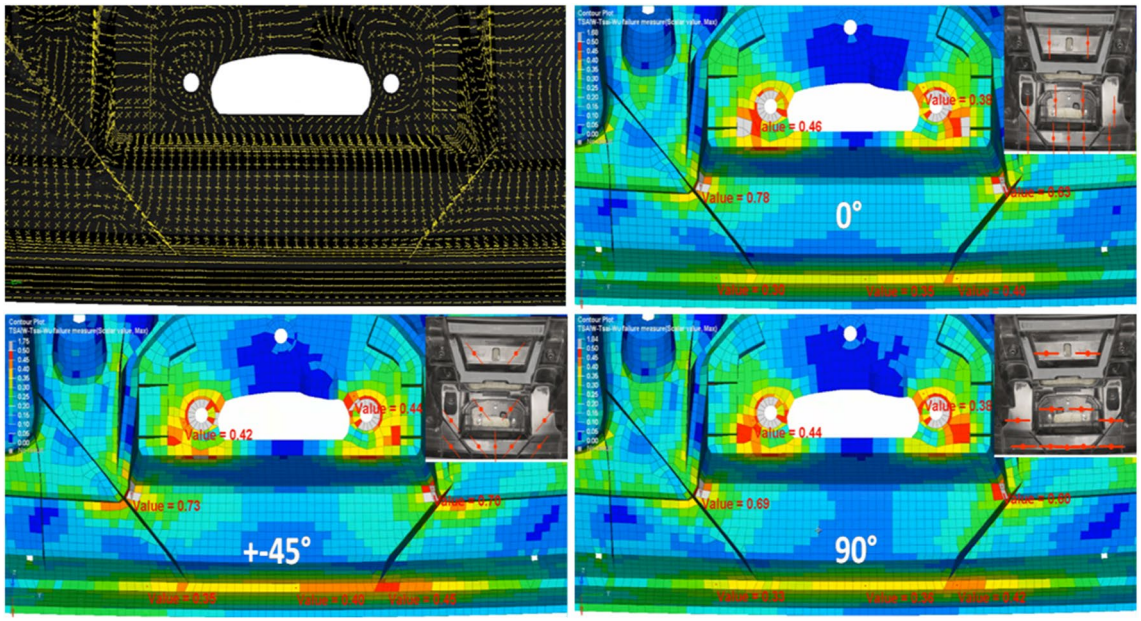

Fig. 17 Effect of the orientation spatial distribution on the failure criterion for $10.^5$ cycles (37.5% thickness reduction)

Fig. 18 Effect of spatial orientation distribution on fatigue criterion and stress state

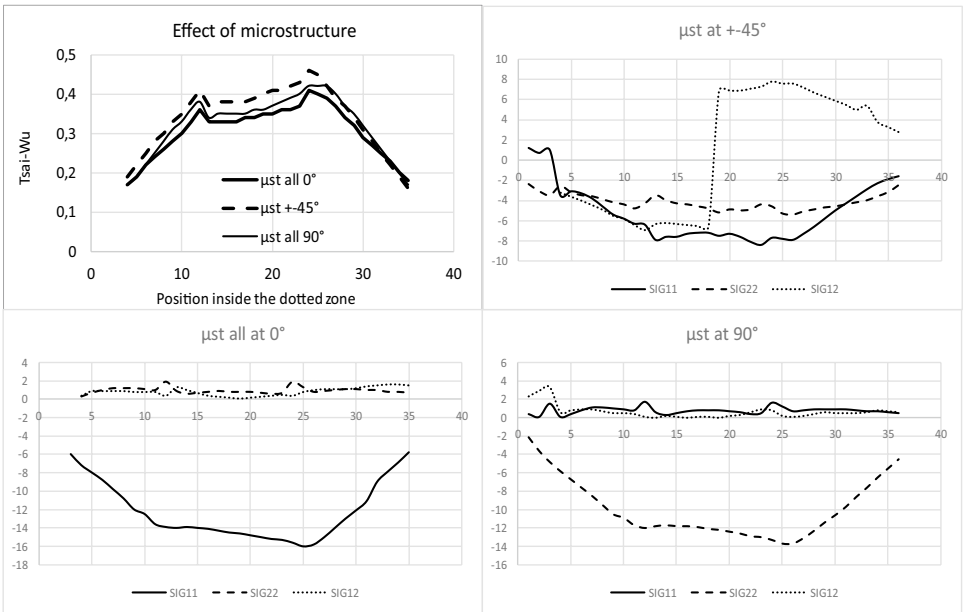

abacus. This tool provides access to Tsai-Wu parameters for any given microstructure and aids in tracking Tsai-Wu criterion evolution during cyclic loading, particularly in critical areas like the lock fixation zone of a tailgate (PSA 3008) subjected to repeated impact.

Our newly developed tool not only visualizes the spatial distribution of the failure criterion during fatigue but also proves highly effective in optimizing short fiber composite components, notably in weight reduction. Interestingly, our analysis demonstrates that reducing thickness can exponentially impact component fatigue life. Additionally, our investigation into the spatial distribution of fiber orientation challenges conventional beliefs; altering fiber orientation does not consistently influence fatigue failure due to stress reorientation from these changes.

These findings hold significant implications for practical design, challenging established norms in continuous fiber composites. Contrary to the belief that aligning fibers with the maximum principal stress direction improves fatigue strength, our work highlights its inapplicability in short fiber composites where the matrix plays a crucial role. In essence, our approach serves as an advanced micromechanical finite

element tool for the fatigue design of multi-microstructured short fiber reinforced composite structures.

In practical terms, our micro-mechanical method opens avenues for the automotive industry to substantially reduce vehicle weight, thereby conserving energy and curbing greenhouse gas emissions. Notably, it showcases potential in optimizing component thickness, as evidenced in the PSA 3008 tailgate. We propose further coupling our approach with software capable of predicting the spatial distribution of microstructures within structures, thus enhancing its utility.

Moreover, our approach generates a comprehensive database across all scales. Looking ahead, employing a machine learning approach to optimize parameters in designing and using composite structures with discontinuous reinforcement stands as a potential future direction. This avenue holds promise for future advancements in this domain.

Author contribution JF, MAL, and MS: construct the idea. JF, SN, KB, MAL, AK, RTB, and MS: analyzed results, draft manuscript preparation, and wrote the paper. JF, SN, KB, MAL, AK, RTB, and MS: corrected the English and the paper format.

Data availability The authors declare that the data and the materials of this study are available within the article.

Declarations

Consent to participate Not applicable.

Consent for publication Not applicable.

Conflict of interest The authors declare no competing interests.

References

1. Hangs B, Bücheler D, Karcher M, Henning F (n.d.) High-volume production of structural automobile parts: comparative study of relevant com
2. Bruderick M, Denton D, Shinedling M (2013) Applications of carbon fiber SMC for the dodge viper. Proceedings to Automotive Composites Conference & Exhibition (ACCE), Detroit
3. Yang X, Liu L, Wang Y (2022) Random fatigue life prediction of automobile lower arm via modified Corten–Dolan model. Fatigue Fract Eng Mater Struct
4. Shirinbayan M, Fitoussi J, Abbasnezhad N, Meraghni F, Surowiec B, Tcharkhtchi A (2017) Mechanical characterization of a low density sheet molding compound (LD-SMC): multi-scale damage analysis and strain rate effect. Compos Part B 131
5. Bernasconi A, Cosmi F, Dreossi D (2008) Local anisotropy analysis of injection moulded fiber reinforced polymer composites. Compos Sci Technol 68:2574–2581
6. Meraghni F, Benzeggagh ML (1995) Micromechanical modelling of matrix degradation in randomly oriented discontinuous-fibre composites. Compos Sci Technol 55(2):171–186. https://doi.org/10.1016/0266-3538(95)00096-8
7. Jendli Z, Meraghni F, Fitoussi J, Baptiste D (2004) Micromechanical analysis of strain rate effect on damage evolution in sheet molding compound composites. Compos Appl Sci Manuf 35(7–8):779–785. https://doi.org/10.1016/j.compositesa.2004.01.020
8. Ben CheikhLarbi A, Sai K, Sidhom H, Baptiste D (2006) Constitutive model of micro-mechanical damage to predict reduction in stiffness of a fatigued SMC composite. J Mater Eng Perform 15(5):575–580. https://doi.org/10.1361/105994906X124569
9. Fitoussi J, Bocquet M, Meraghni F (2013) Effect of the matrix behavior on the damage of ethylene-propylene glass fiber reinforced composite subjected to high strain rate tension. Compos B Eng 45(1):1181–1191. https://doi.org/10.1016/j.compositesb.2012.06.011
10. Fitoussi J, Meraghni F, Jendli Z, Hug G, Baptiste D (2005) Experimental methodology for high strain-rates tensile behaviour analysis of polymer matrix composites. Compos Sci Technol 65(14):2174–2188. https://doi.org/10.1016/j.compscitech.2005.05.001
11. Jendli Z, Fitoussi J, Meraghni F, Baptiste D (2005) Anisotropic strain rate effects on the fibre-matrix interface decohesion in sheet moldingcompound composites. Compos Sci Technol 65(3–4):387–393. https://doi.org/10.1016/j.compscitech.2004.09.027
12. Shirinbayan M, Fitoussi J, Meraghni F, Surowiec B, Bocquet M, Tcharkhtchi A (2015) High strain rate visco-damageable behavior of advanced sheet molding compound (A-SMC) under tension. Compos B Eng 82:30–41. https://doi.org/10.1016/j.compositesb.2015.07.010
13. Al Jahwari F, Naguib HE (2016) Finite element creep prediction of polymeric voided composites with 3D statistical-based equivalent microstructure reconstruction. Compos Part B 99
14. Ren M, Cong J, Wang Bo, Wang L (2018) Extended multiscale finite element method for large deflection analysis of thin-walled composite structures with complicated microstructure characteristics. Thin-Walled Structures 130:273–285. https://doi.org/10.1016/j.tws.2018.05.021
15. Fitoussi J, Bourgeois N, Guo G, Baptiste D (1996) Prediction of the anisotropic damaged behavior of composite materials: introduction of multilocal failure criteria in a micro-macro relationship. Comput Mater Sci 5:87–100. https://doi.org/10.1016/0927-0256(95)00061-5
16. Fitoussi J, Guo G, Baptiste D (1996) Determination of a tridimensional failure criterion at the fibre/matrix interface of an organic-matrix/discontinuous-reinforcement composite. Compos Sci Technol 56(7):755–760. https://doi.org/10.1016/0266-3538(96)00017-6
17. Fitoussi J, Guo G, Baptiste D (1998) A statistical micromechanical model of anisotropic damage for S.M.C. composites. Compos Sci Technol 58(5):759–763. https://doi.org/10.1016/S0266-3538(97)00163-2
18. Meraghni F, Blakeman CJ, Benzeggagh ML (1996) Effect of interfacial decohesion on stiffness reduction in a random discontinuous-fibre composite containing matrix microcracks. Compos Sci Technol 56(5):541–555. https://doi.org/10.1016/0266-3538(96)00039-5
19. Derrien K, Fitoussi J, Guo G, Baptiste D (2000) Prediction of the effective damage properties and failure properties of nonlinear anisotropic discontinuous reinforced composites. Comput Meth Appl Mech Eng 185(2–4):93–107. https://doi.org/10.1016/S0045-7825(99)00253-4
20. Desrumaux F, Meraghni F, Benzeggagh ML (2000) Micromechanical modelling coupled to a reliability approach for damage evolution prediction in composite material. Appl Compos Mater 7(4):231–250. https://doi.org/10.1023/A:1008959400978
21. Meraghni F, Desrumaux F, Benzeggagh ML (2002) Implementation of a constitutive micromechanical model for damage analysis in glass mat reinforced composite structures. Compos Sci Technol 62(16):2087–2097. https://doi.org/10.1016/S0266-3538(02)00110-0
22. Desrumaux F, Meraghni F, Benzeggagh ML (2001) Generalised mori-tanaka scheme to model anisotropic damage using numerical

Eshelby tensor. J Compos Mater 35:603–624. https://doi.org/10.1177/002199801772662091
23. Jendli Z, Meraghni F, Fitoussi J, Baptiste D (2009) Multi-scales modelling of dynamic behaviour for discontinuous fibre SMC composites. Compos Sci Technol 69(1):97–103. https://doi.org/10.1016/j.compscitech.2007.10.047
24. Kammoun S, Doghri I, Brassart L, Delannay L (2015) Micromechanical modeling of the progressive failure in short glass-fiber reinforced thermoplastics - first pseudo-grain damage model. Compos Appl Sci Manuf 73:166–175. https://doi.org/10.1016/j.compositesa.2015.02.017
25. Guo G, Fitoussi J, Baptiste D (1997) Modelling of damage behavior of a short-fiber reinforced composite structure by the finite element analysis using a micro-macro law. Int J Damage Mech 6:278–299 (0803973233)
26. Nguyen BN, Khaleel MA (2004) A mechanistic approach to damage in short-fiber composites based on micromechanical and continuum damage mechanics descriptions. Compos Sci Technol 64(5):607–617. https://doi.org/10.1016/S0266-3538(03)00293-8
27. Baptiste D (2003) Nonlinear behavior micromechanical multiscale modelling of discontinuous reinforced composites. Mater Sci Forum 426–432:3939–3944. https://doi.org/10.4028/www.scientific.net/MSF.426-432.3939
28. Yang W, Pan Y, Pelegri AA (2012) Multiscale modeling of matrix cracking coupled with interfacial debonding in random glass fiber composites based on volume elements. J Compos Mater 47(27):3389–3399. https://doi.org/10.1177/0021998312465977
29. Notta-Cuvier D, Lauro F, Bennani B (2014) Modelling of progressive fibre/matrix de- bonding in short-fibre reinforced composites up to failure. Int J Solid Struct 66:140–150. https://doi.org/10.1016/j.ijsolstr.2015.03.034
30. Laribi MA, Tamboura S, Fitoussi J, Tié Bi R, Tcharkhtchi A, Ben Dali H (2018) Fast fatigue life prediction of short fiber reinforced composites using a new hybrid damage approach: application to SMC. Compos Part B: Engineering 139:155–162. https://doi.org/10.1016/j.compositesb.2017.11.063
31. Liua X-T, Wanga H-J, Yanga X-B, Laib J-F (n.d.) Prediction and evaluation of fatigue strength via mechanical behavior of materials. J Chin Soc Mech Eng 43(3):229–238
32. De Monte M, Moosbrugger E, Quaresimin M (2010) Influence of temperature and thickness on the off-axis behaviour of short glass fiber reinforced polyamide 6.6–cyclic loading. Compos Part A: Appl Sci Manuf 41(10):1368–79
33. Nouri H, Meraghni F, Lory P (2009) Fatigue damage model for injection-molded short glass fiber reinforced thermoplastics. Int J Fatigue 31(5):934–942
34. Ladèveze P, LeDantec E (1992) Damage modelling of the elementary ply for laminated composites. Compos Sci Technol 43(3):257–267
35. Meraghni F, Nouri H, Bourgeois N, Czarnota C, Lory P (2011) Parameters identification of fatigue damage model for short glass fiber reinforced polyamide (PA6-GF30) using digital image correlation. Proc Eng 10:2110–2116
36. Meftah H, Tamboura S, Fitoussi J, Bendaly H, Tcharkhtchi A (2018) Characterization of a new fully recycled carbon fiber reinforced composite subjected to high strain rate tension, 2017. Appl Compos Mater 25(3):507–526
37. Kachanov LM (1976) On subcritical crack growth. Mech Res Commun 3(1):51–54
38. Laribi MA, Tamboura S, Fitoussi J, Shirinbayan M, Tie Bi R, Tcharkhtchi A, Ben Dali H (n.d.) Microstructure dependent fatigue life prediction for short fibers reinforced composites: application to sheet molding compounds (Submitted in Composites Part B)
39. Ayari H, Fitoussi J, Imaddahen A, Tamboura S, Shirinbayan M, Dali HB, Tcharkhtchi A (2020) Two hybrid approaches to fatigue modeling of advanced-sheet molding compounds (A-SMC) composite. Appl Compos Mater 27(1–2):19–36
40. Zhang L, Liu Z, Wu D, Zhang H, Zhu P (2023) Fast and synergetic fatigue life prediction of short fiber reinforced polymer composites from monotonic and cyclic loading behavior. Compos Sci Technol 241
41. Shirinbayan M, Fitoussi J, Meraghni F, Surowiec B, Laribi M, Tcharkhtchi A (2016) Coupled effect of loading frequency and amplitude on the fatigue behavior of advanced sheet molding compound (A- SMC). J Reinf Plast Compos (JRP)
42. Tamboura S, Sidhom H, Baptiste D (2001) Evaluation de la tenue en fatigue du composite SMC R42. Matériaux et Techniques 3–4:3–11
43. Schemmann M, Görthofer J, Seelig T, Hrymak A, Böhlke T (2018) Anisotropic meanfield modeling of debonding and matrix damage in SMC composites. Compos Sci Technol 161:143–158. https://doi.org/10.1016/j.compscitech.2018.03.041
44. Baney JM, Zhao YH, Weng GJ (1996) Progressive debonding of aligned oblate inclusions and loss of stiffness in a brittle matrix composite. Eng Fract Mech 53:897–910. https://doi.org/10.1016/0013-7944(95)00211-1
45. Zairi F, Nait-Abdelaziz M, Gloaguen JM, Bouaziz A, Lefebvre J-M (2008) Micromechanical modelling and simulation of chopped random fiber reinforced polymer composites with progressive debonding damage. Int J Solids Struct 45:5220–5236
46. Formica G, Lacarbonara W (2013) Damage model of carbon nanotubes debonding in nanocomposites. Compos Struct 96:514–525. https://doi.org/10.1016/j.compstruct.2012.08.049
47. Mori T, Tanaka K (1973) Average stress in matrix and average elastic energy ofmaterials with misfitting inclusions. Acta Metall 21:571–574
48. Li S, Sitnikova E (2018) A critical review on the rationality of popular failure criteria for composites. Compos Commun 8:7–13. https://doi.org/10.1016/j.coco.2018.02.002
49. Mortazavian S, Fatemi A (2015) Fatigue behavior and modeling of short fiber reinforced polymercomposites including anisotropy and temperature effects. Int J Fatigue 77:12–27